Mechanotransducer Piezo1 drives ventilator-induced lung injury in lung epithelial cells via the calcineurin/NFATc3 pathway

MIN LI, SHU-LI ZHANG, FENG YUAN and DAN FENG

Department of Pain Management, Wuhan Hospital of Traditional Chinese and Western Medicine, Wuhan, Hubei 430000, P.R. China

Received November 28, 2025; Accepted February 23, 2026

DOI: 10.3892/mmr.2026.13893

Abstract. Ventilator-induced lung injury (VILI) is a serious complication of mechanical ventilation (MV). The mechanosensitive ion channel Piezo1 converts mechanical forces into biochemical signals; however, its specific role in the pathogenesis of VILI remains unclear. The present study aimed to investigate the role of Piezo1 in lung epithelial cells in mediating VILI and its downstream signalling mechanisms. To this end, the current study utilized a murine VILI model established by high tidal volume MV, lung epithelial-specific *Piezo1* knockout mice, and *in vitro* cyclic stretch of mouse lung epithelial (MLE-12) cells combined with genetic knockdown or pharmacological inhibition of Piezo1. Immunofluorescence and immunohistochemical analyses revealed that Piezo1 protein expression was significantly upregulated in the lung epithelium *in vivo*. Lung epithelial-specific *Piezo1* knockout mice exhibited markedly attenuated MV-induced lung injury, barrier dysfunction and inflammatory responses. *In vitro*, cyclic mechanical stretch similarly upregulated Piezo1 expression in mouse lung epithelial MLE-12 cells, accompanied by cytoskeletal disruption, and release of proinflammatory cytokines IL-6, TNF-α and IL-1β, as assessed using ELISA. Genetic knockdown or pharmacological inhibition of *Piezo1* effectively alleviated these injury phenotypes. Mechanistically, Piezo1 activation mediated stretch-induced Ca^{2+} influx, which triggered calcineurin activation and subsequent nuclear translocation of the transcription factor NFATc3, ultimately driving the release of proinflammatory cytokines, including IL-6, TNF-α and IL-1β. In conclusion, the results of the present study revealed a novel Piezo1/Ca^{2+}/calcineurin/NFATc3 signalling axis that drives pulmonary epithelial inflammation and barrier dysfunction in VILI, suggesting that Piezo1 and its downstream signalling molecules are potential therapeutic targets.

Correspondence to: Professor Dan Feng, Department of Pain Management, Wuhan Hospital of Traditional Chinese and Western Medicine, 215 Zhongshan Avenue, Qiaokou, Wuhan, Hubei 430000, P.R. China
E-mail: fengdan_pain@126.com

Key words: lung injury, mechanical ventilation, lung epithelial cells, Piezo

Introduction

Mechanical ventilation (MV) is essential for respiratory support and employs positive pressure to overcome airway resistance and lung elasticity, inevitably causing pulmonary stretching and strain (1). While necessary for homeostasis, excessive mechanical forces during MV [such as high tidal volumes (HTVs)] trigger epithelial dysfunction (2,3). This maladaptive response, termed 'biotrauma', involves the release of cytokines, such as IL-6, TNF-α and IL-1β, which exacerbates local damage, potentially leading to systemic inflammation and multiple organ failure, collectively known as ventilator-induced lung injury (VILI) (4,5). Key features of VILI include disruption of the lung epithelial barrier, a critical defence mechanism, and pronounced proinflammatory signalling originating from these cells (6,7). However, the precise molecular sensors that translate harmful mechanical stretch into this injurious biochemical response within epithelial cells remain incompletely understood.

Mechanosensitive ion channels translate physical stimuli into biochemical signals within the cellular microenvironment. As the frontline sensors of MV-associated stretch, lung epithelial cells utilize these channels to detect mechanical forces (8). Piezo1 is a ubiquitously expressed, membrane tension-gated, nonselective cation channel activated by forces such as shear stress, compression, stretching and osmotic pressure (9). It is broadly expressed and implicated in diverse physiological and pathophysiological processes, including vascular development and osmoregulation (10). In the lung, Piezo1 is present in epithelial cells and its activation has been linked to processes such as stretch-induced epithelial-mesenchymal transition (11). While other mechanosensors (for example, TRPV4) have been associated with VILI (12,13), the specific role of Piezo1 in mediating inflammatory injury in airway epithelia during MV has not been defined.

It has been hypothesized that Piezo1 may act as a critical mechanotransducer in lung epithelial cells in VILI, orchestrating downstream inflammatory signalling. Therefore, the present study aimed to investigate the role of Piezo1 in lung epithelial cells in VILI, and to elucidate its downstream signalling mechanisms using genetic and pharmacological approaches *in vivo* and *in vitro*.

Materials and methods

Materials and reagents. Cyclosporine A (CsA; cat. no. SML1018) and FK506 (cat. no. F4679) were purchased from MilliporeSigma (Merck KGaA). Myeloperoxidase (MPO) detection kits (cat. no. A044-1-1) were obtained from Nanjing Jiancheng Bioengineering Institute. calcineurin activity assay kits (cat. no. AB139461) were purchased from Abcam. ELISA kits for TNF-α (cat. no. EMC102a), IL-1β (cat. no. EMC001b) and IL-6 (cat. no. EMC004) were acquired from Neobioscience Technology Co., Ltd. The anti-NFATc3 antibody (cat. no. ab245501) was obtained from Abcam and the anti-Piezo1 antibody (cat. no. A23380) was obtained from ABclonal Biotech Co., Ltd. Fluo-3 AM (cat. no. S1056), anti-β-actin (cat. no. AF5003), anti-GAPDH (cat. no. AF1186), anti-Lamin B1 (cat. no. AF1408) and horseradish peroxidase (HRP)-conjugated secondary antibodies (cat. nos. A0208 and A0216) were obtained from Beyotime Biotechnology.

Animals and treatment. A total of 30 male C57BL/6 mice (weight, 20-25 g; age, 6-8 weeks) were procured from Shulaibao (Wuhan) Biotechnology Co., Ltd. The animals were maintained under specific pathogen-free conditions, with a controlled temperature (25˚C), humidity (50±10%) and a 12-h light/dark cycle, with ad libitum access to food and water. The mice were randomly assigned to the sham and HTV groups (n=6/group) using a computer-generated randomization sequence. Histopathological evaluation of lung sections was performed by an investigator who was blinded to the group allocation. A total of 2 mice failed intubation and 1 mouse died during the ventilation protocol; these 3 mice were excluded from the final analysis. All experimental protocols adhered to the guidelines set forth in the National Institutes of Health Guide for the Care and Use of Laboratory Animals (14).

A murine model of VILI was established via MV following a previously described procedure (15). Briefly, anaesthesia was induced by intraperitoneal injection of pentobarbital sodium (50 mg/kg). Following anaesthesia, oral endotracheal intubation was performed using an 18 G catheter, and the mice were ventilated in volume-controlled mode (55-7062; Harvard Apparatus) for 6 h with the following parameters: Tidal volume, 35 ml/kg; respiratory rate, 80 breaths/min; zero positive end-expiratory pressure (HTV group). The fraction of inspired oxygen was maintained at 0.21 throughout. The mice in the sham group underwent intubation and spontaneous breathing for 6 h.

At the end of the experiments, mice were deeply anesthetized with an intraperitoneal injection of sodium pentobarbital (50 mg/kg). Bronchoalveolar lavage fluid (BALF) was collected by cannulating the trachea and instilling 0.4 ml sterile PBS into the left lung three times. Following BALF collection, all mice were euthanized via an intraperitoneal injection of an overdose of sodium pentobarbital (150 mg/kg). Death was confirmed by the cessation of spontaneous breathing and heartbeat, followed by cervical dislocation as a secondary physical method to ensure euthanasia. Immediately after sacrifice, the right lung lobes were harvested separately, the superior lobe was fixed in 4% paraformaldehyde for histopathological analysis, the middle lobe was used for wet-to-dry weight ratio measurement, and the inferior and post-caval lobes were snap-frozen in liquid nitrogen and stored at -80˚C for subsequent MPO activity, western blotting and reverse transcription-quantitative PCR (RT-qPCR) analyses.

Generation of conditional Piezo1 conditional knockout (Piezo1^{CKO}) mice. To establish male mice with tamoxifen-inducible, lung epithelial-specific deletion of *Piezo1* (*Piezo1*^{CKO}), *Piezo1*$^{F/F}$ mice (*Piezo1*$^{tm2.1Apat}$/J; Jackson Laboratory) were bred with Sftpc-Cre^{ERT} mice (Jackson Laboratory) in our laboratory. The resulting offspring were genotyped in our laboratory via PCR with primers targeting the Cre recombinase and the floxed *Piezo1* alleles according to a previously described protocol (10). To induce Piezo1 knockout, 3-week-old *Piezo1*^{CKO} mice (n=20) received daily intraperitoneal injections of tamoxifen (cat. no. HY-13757A; MedChemExpress) dissolved in corn oil (cat. no. HY-Y1888; MedChemExpress) at a concentration of 10 mg/ml (0.1 ml/injection) for 7 consecutive days. Age- and weight-matched *Piezo1*$^{F/F}$ littermates that did not carry the Cre transgene (n=20) were utilized as control animals for the *Piezo1*^{CKO} *mice* cohort. All mice were housed under the same specific pathogen-free conditions as described for the C57BL/6 mice, with controlled temperature (25˚C), humidity (50±10%) and a 12-h light/dark cycle, with *ad libitum* access to food and water. Efficient and specific ablation of Piezo1 in lung epithelial cells was subsequently verified by PCR genotyping and immunofluorescence costaining. Both the control and *Piezo1*^{CKO} mice were subjected to HTV at 8 weeks of age (weight, 22-26 g). Immediately after the 6-h ventilation protocol, the mice were euthanized by intraperitoneal injection of an overdose of sodium pentobarbital (150 mg/kg) followed by cervical dislocation, as described in the aforementioned section, and lung tissues were collected for subsequent analyses.

Cell culture and mechanical stretching. The MLE-12 mouse alveolar epithelial cell line, acquired from the American Type Culture Collection, was cultured in Dulbecco's modified Eagle's medium (cat. no. C11995500BT; Gibco; Thermo Fisher Scientific, Inc.) supplemented with 10% foetal bovine serum (cat. no. 10099141; Gibco; Thermo Fisher Scientific, Inc.) and antibiotics (100 U/ml penicillin and 100 μg/ml streptomycin; cat. no. 15140122; Gibco; Thermo Fisher Scientific, Inc.). The cells were maintained at 37˚C in a humidified atmosphere containing 5% CO_2.

For gene silencing studies, short hairpin (sh)RNA targeting Piezo1 (shPiezo1) and scrambled control shRNA (Scr-shRNA) were designed and synthesized. The shRNA sequences were cloned into the pLKO.1-puro lentiviral vector (cat. no. SHC001; MilliporeSigma). Lentiviral particles were generated using a second-generation packaging system. Briefly, 293T cells (cat. no. CRL-3216; American Type Culture Collection) were co-transfected with the lentiviral transfer plasmid (pLKO.1-shPiezo1 or pLKO.1-Scr; 10 μg), the packaging plasmid psPAX2 (7.5 μg; cat. no. 12260; Addgene, Inc.), and the envelope plasmid pMD2.G (2.5 μg; cat. no. 12259; Addgene, Inc.) using Lipofectamine® 3000 transfection reagent (cat. no. L3000015; Invitrogen; Thermo Fisher Scientific, Inc.) according to the manufacturer's instructions. Transfection was carried out at 37˚C for 6 h, after which the medium was replaced with fresh culture medium. Lentiviral particles were

collected from the supernatant 48 and 72 h post-transfection, to maximize viral yield, filtered through 0.45-μm filters, and concentrated using Lenti-X Concentrator (cat. no. 631232; Takara Bio, Inc.) according to the manufacturer's protocol. The virus pellets were then resuspended in cold culture medium and stored at -80˚C until use.

MLE-12 cells were seeded in 6-well plates at a density of $5x10^5$ cells/well. At 60-70% confluence, MLE-12 cells were transduced with lentiviral particles carrying shPiezo1 or Scr-shRNA in the presence of 8 μg/ml Polybrene (MilliporeSigma) at 37˚C in a humidified 5% CO_2 incubator. The target sequences for the mouse shPiezo1 and Scr-shRNA (negative control) used in the present study are as follows: shPiezo1 (mouse target sequence): 5'-GAGCCAGAAGCT AAGCTGGAA-3'; Scr-shRNA (target sequence): 5'-TTC TCCGAACGTGTCACGT-3'. Lentiviral particles carrying shPiezo1 or Scr-shRNA were used at a multiplicity of infection of 20, with a viral titre of $1x10^8$ TU/ml, as determined by qPCR. A total of 24-48 h post-transduction (to allow for viral genomic integration and expression of the resistance gene), cells were subjected to puromycin selection (2 μg/ml) for 7 days to establish stable cell lines, and maintained in medium containing 0.5 μg/ml puromycin thereafter. Gene silencing efficiency was confirmed using qPCR.

For mechanical stimulation assays, MLE-12 cells were seeded on flexible-bottom 6-well BioFlex plates at $5x10^5$ cells/well and grown to 80% confluence. The culture medium was replaced with fresh medium containing 0.5% foetal bovine serum for 12 h prior to stretching. A Flexcell Tension Plus system (FX-5000 T; Flexcell International Corporation) was employed to apply cyclic stretch (18% elongation, 0.5 Hz, 30 cycles/min) at 37˚C in a humidified atmosphere with 5% CO_2 for the indicated durations (3 or 6 h, or 5-30 min). The peak strain was validated using the calibration loading station of the system prior to the experiments. For calcineurin inhibition experiments, cells were pretreated with CsA (10 μM) or FK506 (10 μM) at 37˚C for 1 h prior to mechanical stimulation. Cells were then subjected to cyclic stretch for 6 h. Non-stretched cells cultured on identical plates served as the sham group.

Histopathological evaluation. The superior lobe of the right lung was fixed in 4% paraformaldehyde at room temperature for 24 h, embedded in paraffin and sectioned at a thickness of 5 μm. Haematoxylin and eosin staining was performed on these sections using haematoxylin (5 min) and eosin (3 min) at room temperature. Stained sections were examined under a light microscope (BX53; Olympus Corporation). Lung injury was assessed using a semi-quantitative scoring system (16) that evaluated four parameters: i) Alveolar congestion, ii) haemorrhage, iii) leukocyte infiltration and iv) alveolar wall thickness, each graded from 0 (normal) to 3 (severe), and the four scores were summed to obtain the total lung injury score (range 0-12).

Analysis of BALF. Following anaesthesia with intraperitoneal injection of pentobarbital sodium (50 mg/kg), the trachea was exposed and cannulated with an 18-gauge needle. The right lung hilum was ligated, and the left lung was consistently lavaged by instilling and withdrawing 0.4 ml sterile PBS three times. Immediately after BALF collection, mice were euthanized by cervical dislocation while maintained under deep anaesthesia. The collected BALF was centrifuged at 400 x g for 10 min at 4˚C. After centrifugation, the cell pellet was resuspended in PBS and total cell counts were determined using a haemocytometer under a light microscope. The results are expressed as the total number of cells per ml of BALF. The protein concentration in the BALF supernatant was quantified using a bicinchoninic acid (BCA) protein assay kit (Beyotime Biotechnology).

Assessment of pulmonary oedema. The wet weight of the right middle lung lobe was recorded immediately after excision. The tissue was then dried at 80˚C for 48 h to obtain the dry weight. The wet/dry weight ratio was calculated to evaluate lung oedema.

Measurement of MPO activity. The inferior lung lobe was homogenized in PBS and centrifuged at ~30,000 x g for 30 min at 4˚C. MPO activity in the supernatant was determined using a commercial MPO assay kit according to the manufacturer's instructions.

Calcineurin activity assay. Lung tissue homogenates or cell lysates were prepared in ice-cold lysis buffer and centrifuged at 12,000 x g for 10 min at 4˚C. The supernatants were collected, and protein concentrations were determined using a bicinchoninic acid (BCA) protein assay kit (Beyotime Biotechnology). Calcineurin activity was then assessed based on the release of inorganic phosphate from the synthetic phosphopeptide substrate RII (DLDVPIPGRFDRRVSVAAE) in the presence of calmodulin. The reaction mixture (containing the sample, RII peptide and calmodulin) was incubated at 30˚C for 30 min and the reaction was terminated by adding molybdate reagent. The absorbance was then measured at 636 nm using a microplate reader (Synergy Neo HTS; BioTek; Agilent Technologies, Inc.). Results were expressed as units per milligram of protein (U/mg protein), where one unit represents the release of 1 μmol phosphate/min.

Intracellular calcium imaging. Cytosolic Ca^{2+} levels were monitored using a Fluo-3 AM fluorescent probe according to the manufacturer's guidelines. After mechanical stimulation, the cells were harvested, washed with PBS and incubated with 5 μM Fluo-3 AM in serum-free medium at 37˚C for 30 min. For fluorescence imaging, cells loaded with Fluo-3 AM were visualized under a fluorescence microscope (IX73; Olympus Corporation) at the indicated time points, and representative images were captured and analysed. For agonist experiments, cells were loaded with Fluo-3 AM as aforementioned, then treated with the Piezo1 agonist Yoda1 (10 μM; cat. no. 5586; Tocris Bioscience) at 37˚C. Fluorescence intensity was measured at 5, 15 and 30 min after Yoda1 treatment using a microplate reader (Synergy Neo HTS). For inhibitor experiments, cells were pretreated with the Piezo1 inhibitor GsMTx4 (5 μM; cat. no. ab141871; Abcam) at 37˚C for 30 min prior to mechanical stimulation. Cells were then subjected to mechanical stretch for 30 min, and intracellular Ca^{2+} levels were measured using a microplate reader (Synergy Neo HTS). The fluorescence values are expressed as $\Delta F/F_0$, where F_0 is the baseline fluorescence prior to stimulation.

Cytokine concentration measurements. The concentrations of TNF-α, IL-6 and IL-1β in the BALF and cell culture supernatants were measured using commercially available ELISA kits according to the manufacturer's protocols. Samples and standards were incubated for 2 h (TNF-α) or 4 h (IL-6, IL-1β) at room temperature. The detection limits of the assays were 4 pg/ml for TNF-α, 2 pg/ml for IL-6 and 1 pg/ml for IL-1β.

Western blotting. Cytoplasmic and nuclear protein extracts were prepared from cultured MLE-12 cells using a commercial extraction kit (Beijing Solarbio Science & Technology Co., Ltd.). Protein concentrations were determined using a BCA protein assay kit, according to the manufacturer's instructions. Equal amounts of protein (30 μg/lane) were separated by SDS-PAGE on 10% gels and transferred onto polyvinylidene fluoride membranes (MilliporeSigma). The membranes were blocked with 5% non-fat milk in Tris-buffered saline containing 0.1% Tween-20 (TBST) at room temperature for 1 h. Subsequently, the membranes were incubated overnight at 4˚C with primary antibodies against Piezo1 (1:500), NFATc3 (1:500), β-actin (1:1,000), GAPDH (1:1,000) and Lamin B1 (1:1,000). GAPDH was used as the loading control for whole-cell lysates, whereas β-actin and Lamin B1 served as loading controls for cytoplasmic and nuclear fractions, respectively. After washing with TBST, the membranes were incubated with HRP-conjugated secondary antibodies (1:5,000) at room temperature for 1 h. Protein bands were visualized using an enhanced chemiluminescence detection reagent (Beyotime Biotechnology) and band intensity was semi-quantified using ImageJ software (version 1.53; National Institutes of Health).

RT-qPCR. Total RNA was isolated from cells using TRIzol reagent (Invitrogen; Thermo Fisher Scientific, Inc.). cDNA synthesis was performed using the PrimeScript™ RT reagent Kit with gDNA Eraser (Takara Bio, Inc.) according to the manufacturer's protocol (RT at 37˚C for 15 min, followed by enzyme inactivation at 85˚C for 5 sec). qPCR was carried out using TB Green® Premix Ex Taq™ (Tli RNaseH Plus) (cat. no. RR420A; Takara Bio, Inc.) on an Applied Biosystems 7500 Fast Real-Time PCR System (Applied Biosystems; Thermo Fisher Scientific, Inc.). The thermocycling conditions were as follows: Initial denaturation at 95˚C for 30 sec, followed by 40 cycles at 95˚C for 5 sec and 60˚C for 34 sec. A dissociation curve analysis was performed at the end of each run to verify specific amplification. The primer sequences were as follows: Mouse *Piezo1*, forward 5'-TCATCATCCTTA ACCACATGGTG-3', reverse 5'-TGAAGACGATAGCTGTCA TCCA-3'; mouse *Gapdh*, forward 5'-AGGTCGGTGTGAACG GATTTG-3', reverse 5'-TGTAGACCATGTAGTTGAGGT CA-3'. Relative gene expression was analysed using the $2^{-\Delta\Delta Cq}$ method (17), with GAPDH serving as the internal control.

Immunohistochemical analysis. Lung tissue samples were fixed in 4% paraformaldehyde at room temperature for 24 h, embedded in paraffin and sectioned at a thickness of 5 μm. After deparaffinization and rehydration, antigen retrieval was performed by heating the sections in citrate buffer (pH 6.0) at 95˚C for 20 min. Endogenous peroxidase activity was blocked by incubating the sections with 3% hydrogen peroxide in methanol for 10 min at room temperature, and the sections were then incubated with 5% normal goat serum (cat. no. S-1000; Vector Laboratories; Maravai LifeSciences) in PBS for 1 h at room temperature to block non-specific binding sites.

The sections were then incubated overnight at 4˚C with primary antibody against Piezo1 (1:200). After washing with PBS, the sections were incubated with biotin-conjugated goat anti-rabbit IgG secondary antibody (1:200; cat. no. BA-1000; Vector Laboratories; Maravai LifeSciences) for 30 min at room temperature, followed by incubation with streptavidin-horseradish peroxidase conjugate (1:500; cat. no. SA-5004; Vector Laboratories; Maravai LifeSciences) for 30 min at room temperature. Immunoreactivity was visualized using DAB substrate kit (cat. no. SK-4100; Vector Laboratories; Maravai LifeSciences) according to the manufacturer's instructions. Sections were counterstained with hematoxylin room temperature for 5 min, dehydrated through graded ethanol and xylene, and mounted with permanent mounting medium. Stained sections were examined under a light microscope (BX53) and images were captured using Olympus CellSens Imaging software (version 1.16; http://www.olympus-lifescience.com/en/software/cellsens/).

Immunofluorescence staining

Lung tissue sections staining. Lung tissue samples were fixed in 4% paraformaldehyde at room temperature for 24 h, embedded in paraffin and sectioned at a thickness of 5 μm. After deparaffinization and rehydration, antigen retrieval was performed by heating the sections in citrate buffer (pH 6.0) at 95˚C for 20 min. The sections were then permeabilized with 0.3% Triton X-100 in PBS for 10 min at room temperature and blocked with 5% normal goat serum in PBS for 1 h at room temperature. The sections were incubated overnight at 4˚C with rabbit anti-Piezo1 primary antibody (1:200) and mouse anti-cytokeratin 8 primary antibody (CK8; 1:200; cat. no. ab9023; Abcam). After washing with PBS, the sections were incubated with Alexa Fluor 488-conjugated goat anti-mouse IgG (1:500; cat. no. A11001; Invitrogen; Thermo Fisher Scientific, Inc.) and Alexa Fluor 594-conjugated goat anti-rabbit IgG (1:500;cat. no. A11012; Invitrogen; Thermo Fisher Scientific, Inc.) for 1 h at room temperature in the dark. Nuclei were counterstained with DAPI (1 μg/ml; cat. no. C1005; Beyotime Biotechnology) for 5 min at room temperature. Stained sections were mounted with anti-fade mounting medium and visualized under a confocal laser scanning microscope (Zeiss LSM 880; Zeiss AG). Images were captured and analysed using Zeiss Zen 2011 software (https://www.zeiss.com.cn/microscopy/products/microscope-software/zen.html).

Cultured cell staining. MLE-12 cells seeded on coverslips at a density of $5x10^5$ cells per well in 6-well plates, then fixed with 4% paraformaldehyde for 15 min at room temperature, permeabilized with 0.3% Triton X-100 in PBS for 10 min and blocked with 5% normal goat serum in PBS for 1 h at room temperature. For F-actin staining, cells were incubated with FITC Phalloidin (1:200; cat. no. RM02836; ABclonal Biotech Co., Ltd.) for 30 min at room temperature in the dark. For NFAT isoform detection, cells were incubated overnight at 4˚C with primary antibodies against NFATc1 (1:100; cat. no. ab2796; Abcam), NFATc2 (1:100; cat. no. ab2722; Abcam), NFATc3 (1:100) or NFATc4 (1:100; cat. no. ab99431;

Abcam). After washing, cells were incubated with Alexa Fluor 594-conjugated goat anti-rabbit IgG (1:500; cat. no. A11012; Invitrogen; Thermo Fisher Scientific, Inc.) for 1 h at room temperature in the dark. Nuclei were counterstained with DAPI (1 μg/ml) for 5 min. Coverslips were mounted onto glass slides with anti-fade mounting medium and visualized under a confocal laser scanning microscope (Zeiss LSM 880). Images were captured and analysed using ZEN software.

Statistical analysis. Data were analysed using GraphPad Prism 7.04 (Dotmatics). Normality was assessed using the Shapiro-Wilk test. For comparisons between two groups, normally distributed continuous data were analysed using an unpaired Student's t-test and are presented as the mean ± SD. By contrast, nonnormally distributed continuous data or ordinal data (for example, lung injury score) were analysed using the Mann-Whitney U test and are presented as the median with interquartile range (IQR). For experiments involving more than two groups, oneway analysis of variance (ANOVA) followed by Bonferroni's post hoc test was used for normally distributed data, whereas the Kruskal-Wallis test followed by Dunn's post hoc test was applied for nonnormally distributed or ordinal data. For factorial designs with two independent factors (for example, genotype and ventilation status), twoway ANOVA followed by Bonferroni's post hoc test was performed. P<0.05 was considered to indicate a statistically significant difference. All experiments included at least six biological replicates per group.

Results

Piezo1 expression is upregulated in lung epithelium during VILI in vivo and in vitro. To investigate the potential association between Piezo1 protein abundance and VILI, immunofluorescence staining for Piezo1 was performed on lung sections from experimental mice. Immunofluorescence analysis revealed constitutive expression of Piezo1 in the lung epithelium of sham-operated control mice, as evidenced by its colocalization with the epithelial marker CK8 (Fig. 1A). Notably, compared wiin the sham control mice, mice subjected to 6 h of HTV MV exhibited a marked increase in Piezo1 immunofluorescence intensity within the lung epithelium. In line with these findings, immunohistochemical analysis revealed a clear increase in Piezo1 protein expression in the lung tissue of mice exposed to MV (Fig. 1B).

Consistent with the established VILI pathology, histopathological evaluation revealed that ventilation with HTV induced marked lung injury, as evidenced by alveolar wall thickening, inflammatory cell infiltration, alveolar congestion and haemorrhage in lung tissue sections (Fig 1C) The lung injury score was significantly elevated in the HTV group [median (IQR): 5.60 (4.83-6.50)] compared with in the sham group [2.25 (1.60-3.13) (P<0.01; Fig. 1C and D). Barrier dysfunction was evidenced by a ~2.4-fold increase in BALF protein concentration (813.8±51.63 vs. 335.7±45.48 μg/ml in the sham group; P<0.05; Fig. 1E), and a ~2.7-fold increase in the total BALF cell count (P<0.05; Fig. 1F). The lung wet/dry weight ratio, indicating oedema, was greater in mice in the HTV group (5.44±0.64) compared with that in sham mice (3.98±0.54; P<0.05; Fig. 1G). Inflammatory marker levels were also elevated in the HTV group: Lung tissue MPO activity increased by ~2.6-fold (P<0.01), whereas the BALF levels of IL-6, TNF-α, and IL-1β were increased by ~4.7-, 5.6- and 3.1-fold, respectively (all P<0.001 vs. sham; Fig. 1H-K).

The current study also assessed whether mechanical stress could directly upregulate Piezo1 expression in lung epithelial cells *in vitro*. Compared with in control cells, MLE-12 cells subjected to mechanical stretch (18% elongation, 0.5 Hz) exhibited a time-dependent increase in Piezo1 mRNA expression, which was upregulated ~3.2-fold at 3 h and ~6.5-fold at 6 h (both P<0.001; Fig. 2A). The protein levels followed a similar trend, increasing by ~1.4-fold at 3 h and ~2.0-fold at 6 h post-stretching (P<0.05 and P<0.001, respectively; Fig. 2B and C). Concomitantly, after 6 h of stretch-induced epithelial injury, the F-actin cytoskeleton was notably disrupted (Fig. 2D), and the levels of IL-6, TNF-α and IL-1β in the supernatant were increased by ~3.9-, 7.1- and 6.1-fold, respectively (all P<0.001 vs. sham; Fig. 2E-G).

Genetic ablation of epithelial Piezo1 attenuates VILI in vivo. To establish causality, a lung epithelial-specific *Piezo1* knockout mouse model (Piezo1^{CKO}) was used (Fig. 3A). Among ventilated mice, the lung injury score was significantly lower in the Piezo1^{CKO} group than in the Piezo1$^{F/F}$ group [median (IQR): 3.25 (2.95-4.68) vs. 5.80 (5.00-6.58); P<0.05; Fig. 3B and C]. Barrier function was preserved, with the BALF protein concentration decreased by ~53.2% (P<0.001) and the total BALF cell count reduced by ~43.4% (P<0.05) relative to those in the ventilated Piezo1$^{F/F}$ group (Fig. 3D and E). The lung wet/dry weight ratio and MPO activity were also reduced by ~26.1 and 51.1%, respectively (both P<0.001; Fig. 3F and G). Notably, HTV MV-induced elevations in the levels of cytokines (IL-6, TNF-α, and IL-1β) in the BALF were nearly abolished in Piezo1^{CKO} mice, remaining at baseline levels (IL-6 and IL-1β: P<0.05; TNF-α: P<0.01 vs. ventilated Piezo1$^{F/F}$ mice; Fig. 3H-J).

Genetic inhibition of Piezo1 protects against stretch-induced injury in vitro. Compared with in the Scr-shRNA control group, stable knockdown of Piezo1 in MLE-12 cells (shPiezo1) resulted in a 62.1% reduction in mRNA expression and a 78.5% reduction in protein expression (P<0.001; Fig. 4A-C). In the Scr-shRNA cells, 6 h of stretching markedly increased cytokine secretion (IL-6, 6.5-fold; TNF-α, 4.3-fold; IL-1β, 4.0-fold; all P<0.001 vs. unstretched control cells; Fig. 4D-F). This response was almost completely abolished in shPiezo1 cells (all P<0.01 vs. stretched Scr-shRNA cells). Furthermore, while stretching severely disrupted the F-actin network in control cells, cytoskeletal integrity was largely preserved in shPiezo1 cells under identical conditions (Fig. 4G).

Piezo1 mediates mechanical stretch-induced Ca2+ influx and activates calcineurin signalling. Using Fluo-3 AM, initial analysis confirmed that treatment with the Piezo1 agonist Yoda1 for 30 min significantly increased intracellular Ca^{2+} levels to approximately twice the baseline level in control cells (P<0.001; Fig. 5A). Similarly, mechanical stretching increased intracellular Ca^{2+} levels in Fluo-3 AM-loaded MLE-12 cells (Fig. 5B). This Ca^{2+} response was blocked in cells transfected with shPiezo1 (122% of baseline, P<0.001) or by the Piezo1

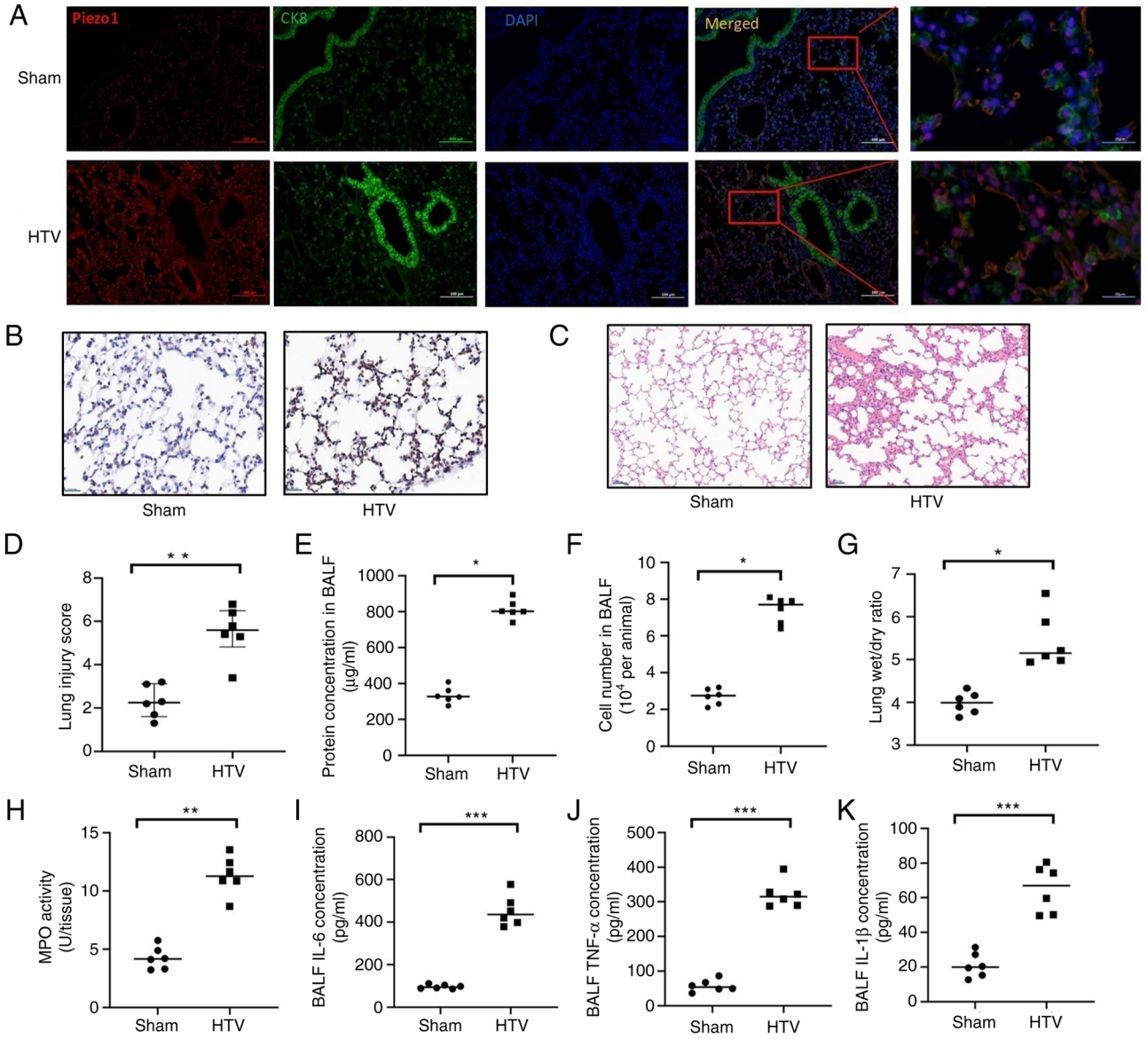

Figure 1. Piezo1 expression is upregulated in the lung epithelium during ventilator-induced lung injury. (A) Representative immunofluorescence images of lung sections from sham-operated control mice and mice subjected to 6 h of mechanical ventilation. Piezo1 protein (red) is constitutively expressed and colocalizes (yellow in merged panels) with the epithelial cell marker CK8 (green). Nuclei were counterstained with DAPI (blue). Scale bar, 100 μm. (B) Representative images of immunohistochemical staining for Piezo1 expression in lung epithelium from sham-operated mice and mice subjected to 6 h of mechanical ventilation. Scale bar, 20 μm (original magnification, x400). (C) Representative haematoxylin and eosin-stained lung sections from sham-operated and HTV-ventilated mice. Scale bar, 50 μm. (D) Quantitative lung injury score was determined based on histological evaluation of alveolar congestion, haemorrhage, leukocyte infiltration and alveolar wall thickness, each graded from 0 (normal) to 3 (severe). Data are presented as the median (interquartile range); n=6 mice/group and Pvalues were determined by Mann-Whitney U test. Lung injury was further evaluated on the basis of (E) protein concentration, (F) cell number in BALF and (G) wet/dry weight ratio. (H) MPO activity in lung tissue. Proinflammatory cytokines in BALF were evaluated using the following ELISA kits: (I) IL-6, (J) TNF-α and (K) IL-β. (E-K) Data are presented as the mean ± SD, n=6 mice/group. Pvalues were determined by Student's t-test. *P<0.05, **P<0.01, ***P<0.001. BALF, bronchoalveolar lavage fluid; CK8, cytokeratin 8; HTV, high tidal volume; MPO, myeloperoxidase.

inhibitor GsMTx4 (5 μM) (peak reduced to 125% of baseline, P<0.001 vs. stretch alone) (Fig. 5C and D).

To elucidate the mechanism by which Piezo1-mediated Ca^{2+} influx regulates epithelial inflammation, the involvement of calcineurin, a Ca^{2+}/calmodulin-dependent serine/threonine phosphatase, was investigated. Stretch increased calcineurin activity by 2.2-fold in control cells (P<0.001), but this increase was reduced to 1.3-fold in cells transfected with shPiezo1 (P<0.001; Fig. 5E). To define the role of calcineurin in Piezo1-dependent inflammation, the pharmacological inhibitors CsA and FK506 were used. Pretreatment with the calcineurin inhibitors CsA or FK506 (both at 10 μM) significantly attenuated mechanical stretch-induced cytokine release, reducing IL-6, TNF-α, and IL-1β levels by 70-85% (all P<0.001; Fig. 5F-H). Furthermore, the notable disruption in the F-actin network of stretched cells was alleviated by the pharmacological inhibitors CsA and FK506 (Fig. 5I).

Piezo1/Ca^{2+}/calcineurin axis drives NFATc3 activation in stretched epithelial cells. The NFAT family consists of five members, first known as transcriptional regulators of T-cell development, maturation and activation. Among these genes,

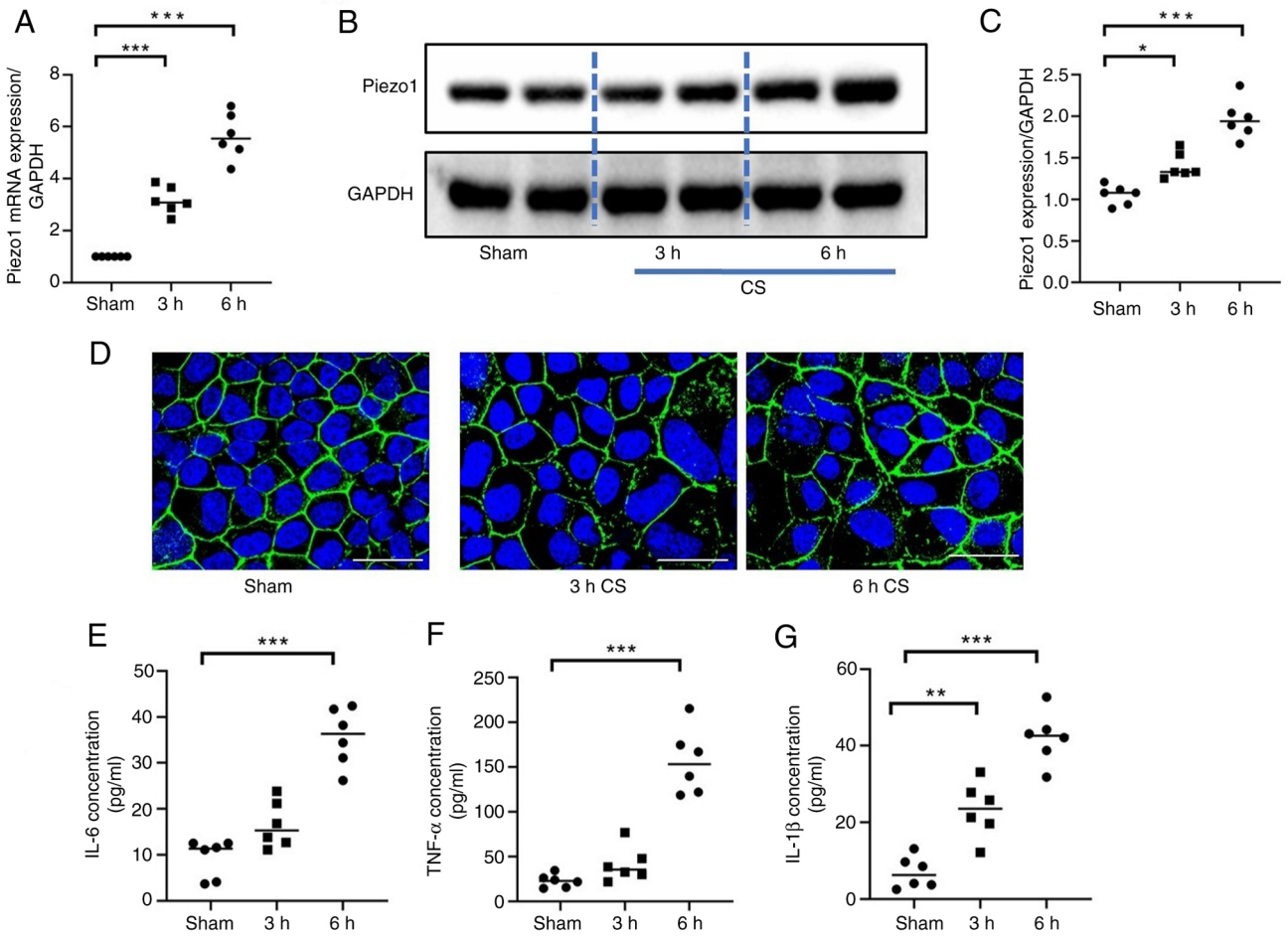

Figure 2. CS induces Piezo1 expression and epithelial injury markers in lung epithelial cells *in vitro*. (A) Representative western blot analysis of Piezo1 protein expression in lung epithelial cells under control (unstretched) conditions, and after 3 or 6 h of CS. (B) Semi-quantification of Piezo1 protein expression normalized to that of GAPDH. (C) Piezo1 mRNA expression in sham and stretched cells (after 3 and 6 h). (D) Representative fluorescence images of F-actin (phalloidin, green) and nuclei (DAPI, blue) in control and stretched cells. Scale bar, 20 μm. Proinflammatory cytokine levels of (E) IL-6, (F) TNF-α and (G) IL-1β protein levels in sham versus stretched cells. Data are presented as the mean ± SD, n=6 each. Pvalues were determined by oneway ANOVA. *P<0.05, **P<0.01, ***P<0.001. CS, cyclic stretch.

NFATc1 to NFATc4 are activated by Ca^{2+}/calcineurin signalling signalling (18). The effects of mechanical stretching on NFAT activation in lung epithelial cells were assessed in the present study by immunostaining with anti-NFAT antibodies. The results revealed that the four isoforms of NFAT were distributed mainly in the cytoplasm of resting cells. Upon mechanical stretch treatment, compared with NFATc1, NFATc2 and NFATc4, NFATc3 exhibited the most pronounced translocation to the nucleus (Fig. 6A). Western blot analysis of nuclear fractions revealed a 2.8-fold increase in nuclear NFATc3 protein expression post-stretching compared with non-stretched control cells (P<0.001), which was prevented by Piezo1 knockdown (1.2-fold; P<0.001 vs. stretched control cells) (Fig. 6B-D). Furthermore, compared with stretching alone, the calcineurin inhibitors CsA and FK506 significantly inhibited mechanical stretch-induced NFATc3 nuclear translocation by 60-75% (P<0.001; Fig. 6E-G).

Discussion

The present study revealed that Piezo1 is an essential mechanotransducer in lung epithelial cells that drives VILI through the activation of a specific Ca^{2+}-dependent signalling cascade. To the best of our knowledge, a previously unrecognized pathway, Piezo1/Ca^{2+}/calcineurin/NFATc3, has been identified, which converts physical stretch into the release of proinflammatory cytokines, such as IL-6, TNF-α and IL-1β, and cytoskeletal disorganization, providing a mechanistic link between mechanical force and the 'biotrauma' of VILI.

The rapid and notable upregulation of Piezo1 expression in lung epithelial cells in response to mechanical stress *in vitro* and *in vivo* observed in the current study suggests the presence of a feed-forward mechanism that amplifies the mechanosensitive response. This is distinct from the role of constitutively active mechanosensors (19) and positions Piezo1 as a master regulator of epithelial maladaptation to excessive stretch. The *in vivo* data demonstrating that epithelial-specific deletion of Piezo1 significantly ameliorated VILI pathology provide compelling evidence for its indispensability. The concordant protective effects of Piezo1 knockdown *in vitro* preserved cytoskeletal integrity and abrogated cytokine production, confirming that the observed benefits are directly attributable to the loss of Piezo1 in epithelial cells rather than indirect systemic effects. These

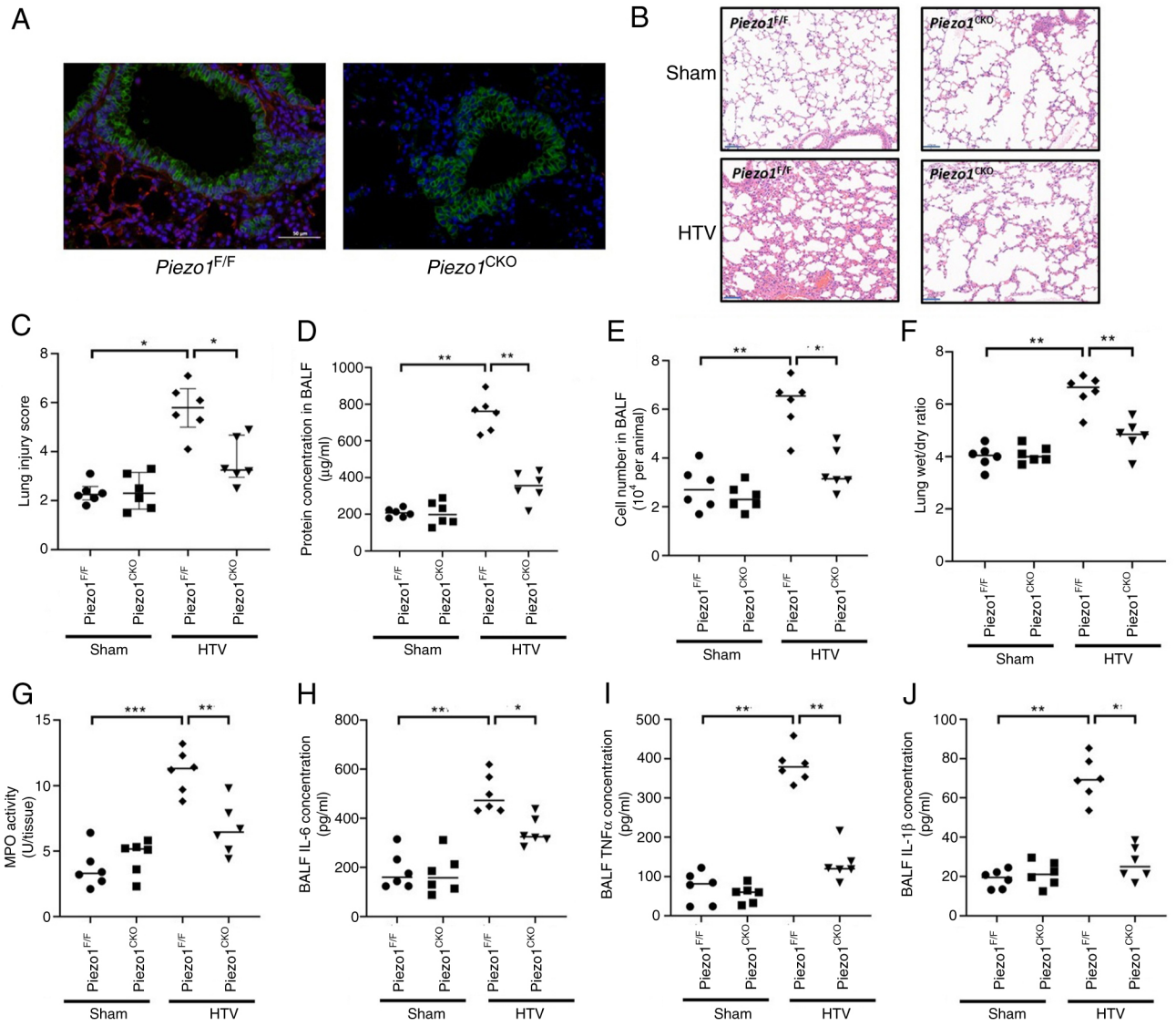

Figure 3. Lung epithelial-specific Piezo1 deletion attenuates ventilator-induced lung injury. (A) Validation of Piezo1 knockout efficiency in the lung epithelium. Representative immunofluorescence images of lung sections from control and Piezo1^{CKO} mice showing the expression of the Piezo1 protein (red), the epithelial cell marker CK8 (green), and nuclei (DAPI, blue). Scale bar, 50 μm. (B) Representative haematoxylin and eosin-stained lung sections from control and Piezo1^{CKO} mice after 6 h of mechanical ventilation. Scale bar, 50 μm. (C) Quantitative histopathological lung injury score. Data are presented as the median (IQR); n=6/group. Data were analysed using the Kruskal-Wallis test followed by Dunn's post hoc test. (D) Total protein concentration in BALF. (E) Total cell counts in the BALF. (F) Lung wet/dry weight ratio. (G) Lung MPO activity. BALF concentrations of the inflammatory cytokines (H) IL-6, (I) TNF-α and (J) IL-1β. (D-J) Data are presented as the mean ± SD, n=6 mice/group. Pvalues were determined by oneway ANOVA. *P<0.05, **P<0.01, ***P<0.001. BALF, bronchoalveolar lavage fluid; CK8, cytokeratin 8; CKO, conditional; HTV, high tidal volume; MPO, myeloperoxidase.

findings align with and markedly extend those of previous studies indicating that Piezo1 is involved in endothelial activation and acute lung injury (20-22) by pinpointing the lung epithelium as a critical site of action.

One key mechanistic insight is the coupling of Piezo1-mediated Ca^{2+} entry to the activation of calcineurin activity (23) and the subsequent nuclear translocation of NFATc3. The moderate Ca^{2+} selectivity of Piezo1 appears uniquely suited to activate calcineurin, a Ca^{2+}/calmodulin-dependent phosphatase that requires sustained, intermediate-level Ca^{2+} signals for its activation (24). This specificity explains why the selective inhibition of Piezo1 was so effective in abrogating the inflammatory response, as it disrupted this precise signalling node. Notably, among the NFAT isoforms, NFATc3 has emerged as the primary responder to mechanical stretch in epithelial cells. This isoform specificity is notable, as it identifies a distinct transcriptional regulator in epithelial mechanoinflammation, differing from the canonical roles of NFATc1/c2 in immune cells (25,26); accordingly, the present data highlight NFATc3 as a key mediator of proinflammatory responses in mechanically stressed epithelial cells. Both Piezo1 knockdown and calcineurin inhibitors completely blocked NFATc3 nuclear translocation, and the production of TNF-α, IL-6 and IL-1β, supporting a linear signalling cascade. These cytokines are established NFAT target genes, and their coordinated upregulation provides a direct molecular explanation for the inflammatory milieu characteristic of VILI.

It is important to contextualize the present findings within the broader literature, which presents a nuanced view of the role of Piezo1 in barrier regulation. For example, Zhong *et al* (21)

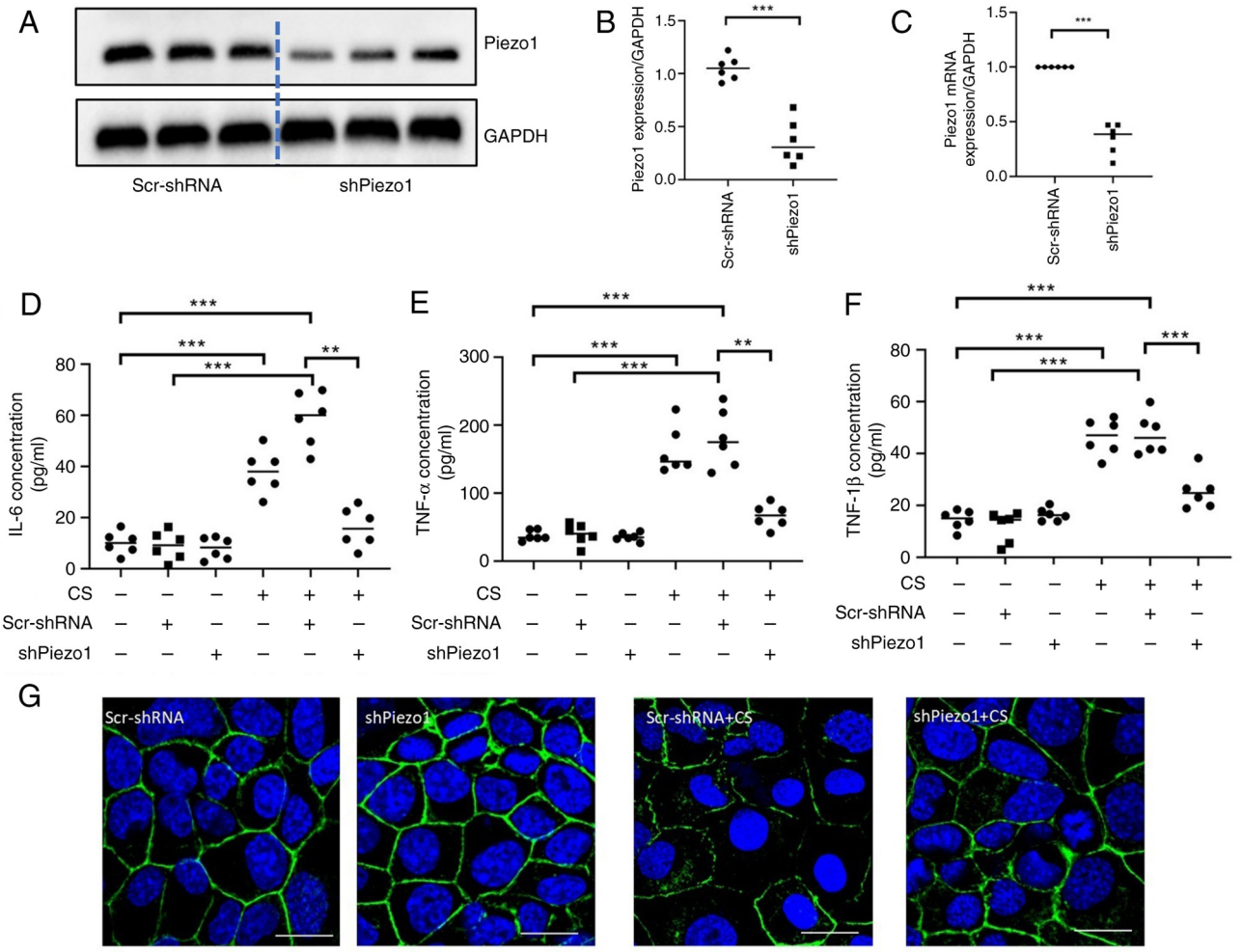

Figure 4. Genetic inhibition of Piezo1 attenuates mechanical stretch-induced cytoskeletal disruption and the inflammatory response in lung epithelial cells *in vitro*. (A) Representative western blotting and (B) semi-quantitative analysis demonstrating efficient knockdown of Piezo1 protein expression in MLE-12 cells transfected with shPiezo1 compared with that in cells transfected with Scr-shRNA. (C) Piezo1 mRNA expression levels measured by quantitative PCR in cells transfected with shPiezo1 compared with those in cells transfected with Scr-shRNA. Proinflammatory cytokine levels in cell culture supernatants from Scr-shRNA and shPiezo1 cells under control conditions or after 6 h of CS: (D) IL-6, (E) TNF-α and (F) IL-1β protein levels. (G) Representative fluorescence images showing F-actin morphology (phalloidin, green) and nuclei (DAPI, blue) in Scr-shPiezo1 and shPiezo1 cells under control (unstretched) conditions or after 6 h of CS. Scale bar, 20 μm. Data are presented as the mean ± SD, n=6 each. Pvalues were determined by oneway ANOVA. **P<0.01, ***P<0.001. CS, cyclic stretch; Scr, scrambled; sh, short hairpin.

suggested that endothelial Piezo1 serves a protective role in maintaining vascular barrier function under alveolar stretch. This apparent contradiction may reflect cell type-specific signalling outcomes, differences in the magnitude or pattern of mechanical stress, or the engagement of distinct downstream effectors. The present data firmly establish an injurious role for epithelial Piezo1 in the context of HTV-induced VILI, underscoring the complexity of mechanosignalling in multicellular organ responses.

From a therapeutic perspective, the protective effects of both genetic and pharmacological Piezo1 inhibition highlight its potential as a novel target. GsMTx4, a selective Piezo1 blocker (27), effectively mitigated injury, suggesting that locally administered Piezo1 inhibitors (such as via nebulization) could serve as a viable adjunctive therapy to lung-protective ventilation. Targeting Piezo1 may offer distinct advantages over broad-spectrum calcium channel blockers because of its restricted expression in specific cell types and its activation mechanism, which is independent of membrane potential, allowing for more selective disruption of pathological mechanosignalling. Furthermore, the current data suggested that targeting the downstream effectors calcineurin and NFATc3 may achieve comparable protection. While the systemic use of calcineurin inhibitors is limited by immunosuppression and toxicity (28), their local delivery to the lungs via inhalation could harness their anti-inflammatory benefits while minimizing systemic side effects (29), a strategy worthy of future exploration.

Despite these advances, several intriguing questions remain. First, the mechanism underlying the rapid transcriptional upregulation of Piezo1 itself by mechanical stretch is unknown. The Hippo pathway effectors YAP and TAZ, which are mechanosensitive transcriptional coactivators, are prime candidates, as they have been shown to bind and regulate the Piezo1 promoter in other contexts (30). Second, the spatial organization of this signalling pathway is likely crucial. It is plausible that Piezo1 channels form signalling nanodomains with calcineurin and possibly other partners

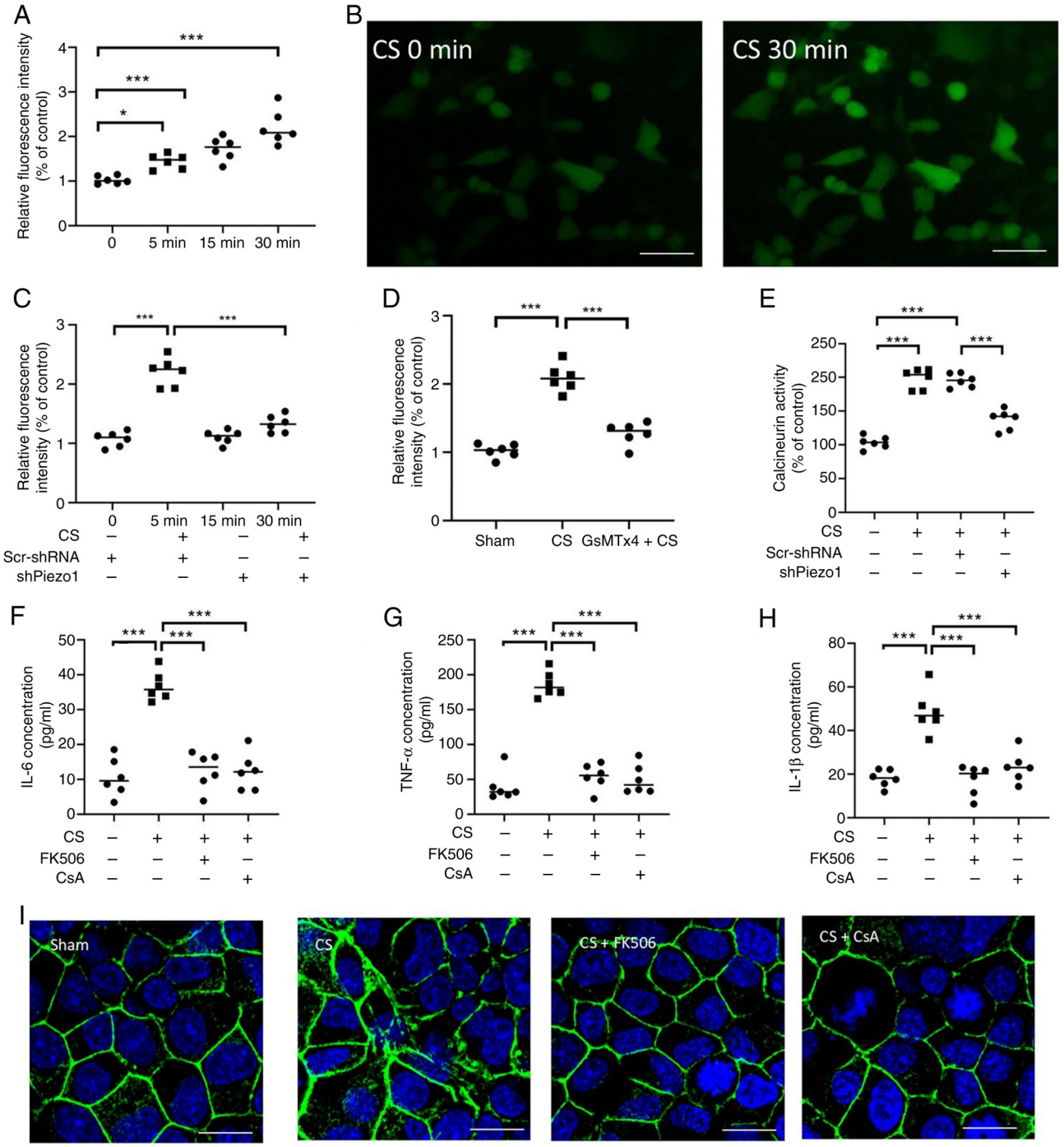

Figure 5. Piezo1 mediates CS-induced Ca^{2+} influx in epithelial cells. (A) Quantitative analysis of cytosolic Ca^{2+} levels ($\Delta F/F_0$) measured using a microplate reader in Fluo-3 AM-loaded MLE-12 cells treated with the Piezo1 agonist Yoda1 (10 μM) for 0, 15 and 30 min. (B) Representative fluorescence microscopy images of Fluo-3 AM-loaded MLE-12 cells at 30 min following the onset of CS Scale bar, 50 μm. (C and D) Both genetic knockdown of Piezo1 (with shPiezo1) and pharmacological inhibition with GsMTx4 (5 μM) attenuated the Ca^{2+} elevation induced by 30-min CS. (E) Genetic knockdown of Piezo1 (with shPiezo1) attenuated mechanical stretch-induced calcineurin activation after 6 h. (F-H) Pharmacological inhibition of calcineurin with CsA (10 μM) or FK506 (10 μM) significantly reduced mechanical stretch -induced cytokine production after 6 h. (I) Disruption of the F-actin network induced by 6-h mechanical stretching was reversed by pretreatment with CsA or FK506. Scale bar, 20 μm. Data are presented as the mean ± SD, n=6 each. Pvalues were determined by oneway ANOVA. *P<0.05, ***P<0.001. CS, cyclic stretch; CsA, cyclosporine A; Scr, scrambled; sh, short hairpin.

near the plasma membrane, facilitating efficient and specific Ca^{2+} transfer. Super-resolution imaging techniques could be employed to visualize this potential 'mechanotransducosome'. Third, the clear preservation of the F-actin cytoskeleton in Piezo1-knockdown cells indicates a dual role for Piezo1 in coordinating both inflammation and structural remodelling. This crosstalk may be mediated through Ca^{2+}-dependent proteases such as calpains, which can cleave cytoskeletal and junctional proteins, and their interplay with integrins warrants further investigation (31). Finally, the relevance of this pathway in human biology must be firmly established. While murine models are invaluable, human lung epithelia may exhibit differences in mechanosensitivity. Validating these findings in more complex human systems, such as primary human

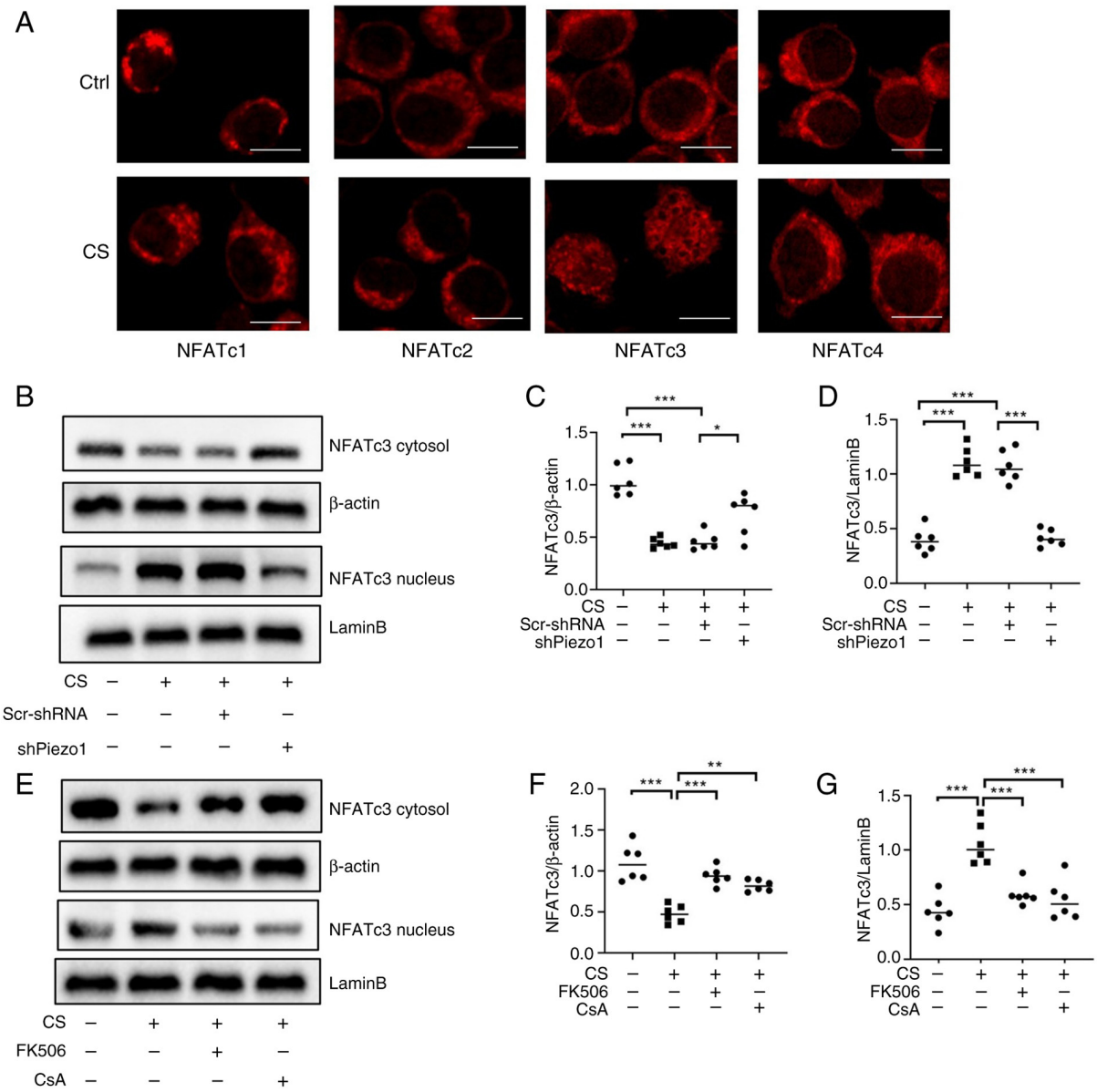

Figure 6. Piezo1 mediates CS-induced inflammation via calcineurin/NFATc3 signalling. (A) Immunofluorescence screening of the nuclear translocation of NFAT isoforms (NFATc1-4) upon CS. NFATc3 showed the most prominent nuclear translocation. Scale bar, 10 μm. (B) Representative western blot images showing NFATc3 protein levels in the nuclear and cytoplasmic fractions of MLE-12 cells transfected with Scr-shRNA or shPiezo1, with or without CS (6 h). GAPDH and Lamin B1 were used as loading controls for cytoplasmic and nuclear fractions, respectively. (C) Semi-quantitative analysis of cytoplasmic NFATc3 protein expression normalized to GAPDH. (D) Semi-quantitative analysis of nuclear NFATc3 protein expression normalized to Lamin B1. (E) Representative western blot images showing NFATc3 protein levels in the nuclear and cytoplasmic fractions of MLE-12 cells treated with or without calcineurin inhibitors (CsA, 10 μM; FK506, 10 μM) prior to CS (6 h). GAPDH and Lamin B1 were used as loading controls for cytoplasmic and nuclear fractions, respectively. (F) Semi-quantitative analysis of cytoplasmic NFATc3 protein expression normalized to GAPDH. (G) Semi-quantitative analysis of nuclear NFATc3 protein expression normalized to Lamin B1. Data are presented as the mean ± SD, n=6 each. Pvalues were determined by oneway ANOVA. *P<0.05, **P<0.01, ***P<0.001. CS, cyclic stretch; CsA, cyclosporine A; Scr, scrambled; sh, short hairpin.

alveolar epithelial cells, lung organoids or precision-cut lung slices, will be a critical step towards clinical translation.

The current management of VILI relies predominantly on limiting tidal volumes and plateau pressures (32). However, VILI still develops in a notable subset of patients, indicating an unmet need for mechanistically targeted therapies (33). The present study indicated that Piezo1 and its downstream signalling molecules are potential targets for pharmacological intervention. Monitoring soluble Piezo1 levels in BALF or serum could be explored as a 'mechanobiological biomarker' to identify patients at high risk for or in the early stages of VILI. Therapeutically, repurposing existing drugs such as calcineurin inhibitors for inhaled delivery, or developing novel Piezo1 antagonists such as optimized versions of GsMTx4, represent promising options. Future research should focus on optimizing the delivery, efficacy and safety of such targeted anti-mechanosensing strategies to complement existing ventilatory protocols and improve outcomes for patients requiring life-supporting MV.

Acknowledgements

Not applicable.

Funding

This work was supported by the Scientific Research Project of Hubei Provincial Health Commission (grant no. WJ2023M123).

Availability of data and materials

The data generated in the present study may be requested from the corresponding author.

Authors' contributions

ML, SLZ and FY performed the experiments. ML and SLZ analysed and interpreted the data. DF contributed to the conception and design of the study and participated in data interpretation. ML and SLZ wrote the original draft. ML, SLZ, FY and DF revised the original draft. DF secured funding. All authors read and approved the final manuscript. ML and DF confirm the authenticity of all the raw data.

Ethics approval and consent for participation

The animal experiments were approved by the Ethics Committee of the Traditional Chinese and Western Medicine Hospital of Wuhan, Tongji Medical College, Huazhong University of Science and Technology (approval no. 2024-103). All procedures adhered to the Guide for the Ethical Review of Animal Welfare (GB/T 35892-2018).

Patient consent for publication

Not applicable.

Competing interests

The authors declare that they have no competing interests.

References

1. Liu G, Dong BB, Ding ZH, Lan C, Zhu CJ and Liu Q: Unphysiological lung strain promotes ventilation-induced lung injury via activation of the PECAM-1/Src/STAT3 signaling pathway. Front Pharmacol 15: 1469783, 2025.
2. Bates JHT, Nieman GF, Kollisch-Singule M and Gaver DP: Ventilator-induced lung injury as a dynamic balance between epithelial cell damage and recovery. Ann Biomed Eng 51: 1052-1062, 2023.
3. Spassov SG, Kessler C, Jost R and Schumann S: Ventilation-like mechanical strain modulates the inflammatory response of BEAS2B epithelial cells. Oxid Med Cell Longev 2019: 2769761, 2019.
4. Slutsky AS and Ranieri VM: Ventilator-induced lung injury. N Engl J Med 369: 2126-2136, 2013.
5. Dolinay T, Himes BE, Shumyatcher M, Lawrence GG and Margulies SS: Integrated stress response mediates epithelial injury in mechanical ventilation. Am J Respir Cell Mol Biol 57: 193-203, 2017.
6. Wang Y, Fang X, Yang Y, Chen L, Xiong W, Song L, Li B, Zhou T, Yu Y, Yang X, *et al*: Death-associated protein kinase 1 promotes alveolar epithelial cell apoptosis and ventilator-induced lung injury through P53 pathway. Shock 57: 140-150, 2022.
7. Englert JA, Macias AA, Amador-Munoz D, Pinilla Vera M, Isabelle C, Guan J, Magaoay B, Suarez Velandia M, Coronata A, Lee A, *et al*: Isoflurane ameliorates acute lung injury by preserving epithelial tight junction integrity. Anesthesiology 123: 377-388, 2015.
8. Solis AG, Bielecki P, Steach HR, Sharma L, Harman CC, Yun S, de Zoete MR, Warnock JN, Toomer SD, Kosenko RA, *et al*: Mechanosensation of cyclical force by PIEZO1 is essential for innate immunity. Nature 573: 69-74, 2019.
9. Fang XZ, Zhou T, Xu JQ, Wang YX, Sun MM, He YJ, Pan SW, Xiong W, Peng ZK, Gao XH and Shang Y: Structure, kinetic properties and biological function of mechanosensitive Piezo channels. Cell Biosci 11: 13, 2021.
10. Wang J, Jing F, Zhao Y, You Z, Zhang A and Qin S: Piezo1: Structural pharmacology and mechanotransduction mechanisms. Trends Pharmacol Sci 46: 752-770, 2025.
11. Fang XZ, Li M, Wang YX, Zhang P, Sun MM, Xu JX, Yang YY, He YJ, Yu Y, Li RT, *et al*: Mechanosensitive ion channel Piezo1 mediates mechanical ventilation-exacerbated ARDS-associated pulmonary fibrosis. J Adv Res 53: 175-186, 2023.
12. Pairet N, Mang S, Fois G, Keck M, Kühnbach M, Gindele J, Frick M, Dietl P and Lamb DJ: TRPV4 inhibition attenuates stretch-induced inflammatory cellular responses and lung barrier dysfunction during mechanical ventilation. PLoS One 13: e0196055, 2018.
13. Li M, Wang Y, Hu Z, Huang S, Chen P, Chen L, Wu J, Wu Z, Yao S and Yang Y: PTEN-mediated senescence of lung epithelial cells drives ventilator-induced pulmonary fibrosis. Theranostics 15: 8360-8376, 2025.
14. National Research Council: Guide for the care and use of laboratory animals. 8th edition. The National Academies Press, Washington, DC, 2011.
15. Li M, Fang XZ, Liu XT, Zheng YF, Xie YB, Ma XD, Xia Y and Shao DH: Inhibition of calcineurin/NFATc4 signaling attenuates ventilatorinduced lung injury. Mol Med Rep 21: 607-614, 2020.
16. Hong W, Zhi FX, Kun TH, Hua FJ, Huan Ling L, Fang F, Wen C, Jie W and Yang LC: 6-Gingerol attenuates ventilator-induced lung injury via anti-inflammation and antioxidative stress by modulating the PPARγ/NF-κB signalling pathway in rats. Int Immunopharmacol 92: 107367, 2021.
17. Livak KJ and Schmittgen TD: Analysis of relative gene expression data using realtime quantitative PCR and the 2 (-Delta Delta C(T)) method. Methods 25: 402-408, 2001.
18. Chaudhry MZ, Borkner L, Kulkarni U, Berberich-Siebelt F and Cicin-Sain L: NFAT signaling is indispensable for persistent memory responses of MCMV-specific CD8+ T cells. PLoS Pathog 20: e1012025, 2024.
19. Wen D, Gao Y, Ho C, Yu L, Zhang Y, Lyu G, Hu D, Li Q and Zhang Y: Focusing on mechanoregulation axis in fibrosis: Sensing, transduction and effecting. Front Mol Biosci 9: 804680, 2022.
20. Jiang L, Zhang Y, Lu D, Huang T, Yan K, Yang W and Gao J: Mechanosensitive Piezo1 channel activation promotes ventilator-induced lung injury via disruption of endothelial junctions in ARDS rats. Biochem Biophys Res Commun 556: 79-86, 2021.
21. Zhong M, Wu W, Kang H, Hong Z, Xiong S, Gao X, Rehman J, Komarova YA and Malik AB: Alveolar stretch activation of endothelial Piezo1 protects adherens junctions and lung vascular barrier. Am J Respir Cell Mol Biol 62: 168-177, 2020.
22. Liang GP, Xu J, Cao LL, Zeng YH, Chen BX, Yang J, Zhang ZW and Kang Y: Piezo1 induced apoptosis of type II pneumocytes during ARDS. Respir Res 20: 118, 2019.
23. Li Z, Jiang Q, Wei J, Dang D, Meng Z and Wu H: Piezo1 promotes the progression of necrotizing enterocolitis by activating the Ca2+/CaMKII-dependent pathway. Commun Biol 8: 417, 2025.
24. Crabtree GR and Olson EN: NFAT signaling: Choreographing the social lives of cells. Cell 109: S67-S79, 2002.
25. Xu T, Keller A and Martinez GJ: NFAT1 and NFAT2 differentially regulate CTL differentiation upon acute viral infection. Front Immunol 10: 184, 2019.
26. Nagai J, Lin J and Boyce JA: Macrophage P2Y6 receptor signaling selectively activates NFATC2 and suppresses allergic lung inflammation. J Immunol 209: 2293-2303, 2022.
27. Wang W, Huang M, Huang X, Ma K, Luo M and Yang N: GsMTx4-blocked PIEZO1 channel promotes myogenic differentiation and alleviates myofiber damage in Duchenne muscular dystrophy. Skelet Muscle 15: 13, 2025.
28. Diker Cohen T, Dotan I, Calvarysky B and Robenshtok E: Endocrine effects of long-term calcineurin inhibitor use in solid organ transplant recipients. Eur J Endocrinol 193: R1-R16, 2025.

29. Neurohr C, Kneidinger N, Ghiani A, Monforte V, Knoop C, Jaksch P, Parmar J, Ussetti P, Sole A, Müller-Quernheim J, *et al*: A randomized controlled trial of liposomal cyclosporine A for inhalation in the prevention of bronchiolitis obliterans syndrome following lung transplantation. Am J Transplant 22: 222-229, 2022.
30. Hasegawa K, Fujii S, Matsumoto S, Tajiri Y, Kikuchi A and Kiyoshima T: YAP signaling induces Piezo1 to promote oral squamous cell carcinoma cell proliferation. J Pathol 253: 80-93, 2021.
31. Nourse JL and Pathak MM: How cells channel their stress: Interplay between Piezo1 and the cytoskeleton. Semin Cell Dev Biol 71: 312, 2017.
32. Acute Respiratory Distress Syndrome Network, Brower RG, Matthay MA, Morris A, Schoenfeld D, Thompson BT and Wheeler A: Ventilation with lower tidal volumes as compared with traditional tidal volumes for acute lung injury and the acute respiratory distress syndrome. N Engl J Med 342: 1301-1308, 2000.
33. Tonetti T, Vasques F, Rapetti F, Maiolo G, Collino F, Romitti F, Camporota L, Cressoni M, Cadringher P, Quintel M and Gattinoni L: Driving pressure and mechanical power: New targets for VILI prevention. Ann Transl Med 5: 286, 2017.